

from substrate-enzyme interactions to stabilize the catalytic transition state (Jencks, 1975). It is our hope that these and other mechanistic studies of PPI will provide the basis for the rational design of therapeutically useful inhibitors of this important enzyme.

REFERENCES

- Acheson, S. A., Barlow, P. N., Lee, G. C., Swanson, M. L., & Quinn, D. M. (1987) *J. Am. Chem. Soc.* 109, 246-252.
- Bromme, D., Beschere, K., Kirschke, H., & Fittkau, S. (1987) *Biochem. J.* 245, 381-385.
- Cleland, W. W. (1975) *Acc. Chem. Res.* 8, 145-151.
- Fersht, A. (1985) *Enzyme Structure and Mechanism*, pp 147-153, W. H. Freeman, New York.
- Fischer, G., Bang, H., & Mech, C. (1984) *Biomed. Biochim. Acta* 43, 1101-1111.
- Fischer, G., Berger, E., & Bang, H. (1989a) *FEBS Lett.* 250, 267-270.
- Fischer, G., Wittmann-Liebold, B., Lang, K., Kiefhaber, T., & Schmid, F. X. (1989b) *Nature* 337, 476-478.
- Gutfreund, H. (1972) *Enzymes: Physical Principles*, p 159, Wiley, New York.
- Handschumacher, R. E., Harding, M. W., Rice, J., Drugge, R. J., & Speicher, D. W. (1984) *Science* 226, 544-547.
- Harding, M. W., Handschumacher, R. E., & Speicher, D. W. (1986) *J. Biol. Chem.* 261, 8547-8555.
- Hirohara, H., Philipp, M., & Bender, M. L. (1977) *Biochemistry* 16, 1573-1580.
- Hogg, J. L., Rodgers, J., Kovach, I. M., & Schowen, R. L. (1980) *J. Am. Chem. Soc.* 102, 79-85.
- Jencks, W. P. (1969) *Catalysis in Chemistry and Enzymology*, McGraw-Hill, New York.
- Jencks, W. P. (1975) *Adv. Enzymol.* 43, 219-404.
- Kovach, I. M., Hogg, J. L., Raben, T., Halbert, K., Rodgers, J., & Schowen, R. L. (1980) *J. Am. Chem. Soc.* 102, 1991-1999.
- Northrop, D. B. (1981) *Annu. Rev. Biochem.* 50, 103-131.
- Ray, W. J. (1983) *Biochemistry* 22, 4625-4637.
- Schowen, K. B. (1978) in *Transition States of Biochemical Processes* (Gandour, R. D., & Schowen, R. L., Eds.) p 225, Plenum Press, New York.
- Sokal, R. R., & Rohlf, F. J. (1981) *Biometry*, 2nd ed., pp 128-137, W. H. Freeman, New York.
- Stein, R. L. (1988) *J. Am. Chem. Soc.* 110, 7907-7908.
- Stein, R. L., Elrod, J. P., & Schowen, R. L. (1983) *J. Am. Chem. Soc.* 105, 2446-2452.
- Stein, R. L., Strimpler, A. M., Hori, H., & Powers, J. C. (1987) *Biochemistry* 26, 1305-1314.
- Takahashi, N., Hayano, T., & Suzuki, M. (1989) *Nature* 337, 473-475.
- Tipton, K. F., & Dixon, H. B. F. (1979) *Methods Enzymol.* 63, 183-234.

Three-Dimensional Structure of Interleukin 8 in Solution[†]

G. Marius Clore,^{*,‡} Ettore Appella,[§] Masaki Yamada,^{||} Kouji Matsushima,[⊥] and Angela M. Gronenborn^{*,‡}
Laboratory of Chemical Physics, National Institute of Diabetes and Digestive and Kidney Diseases, and Laboratory of Cell Biology, National Cancer Institute, National Institutes of Health, Bethesda, Maryland 20892, Laboratory of Molecular Immunoregulation, Biological Response Modifiers Program, Division of Cancer Treatment, National Cancer Institute, Frederick, Maryland 21701-1013, and Research Laboratories, Dainippon Pharmaceutical Company, Suita, Osaka 564, Japan
 Received November 27, 1989; Revised Manuscript Received December 20, 1989

ABSTRACT: The solution structure of the interleukin 8 (IL-8) dimer has been solved by nuclear magnetic resonance (NMR) spectroscopy and hybrid distance geometry-dynamical simulated annealing calculations. The structure determination is based on a total of 1880 experimental distance restraints (of which 82 are intersubunit) and 362 torsion angle restraints (comprising ϕ , ψ , and χ_1 torsion angles). A total of 30 simulated annealing structures were calculated, and the atomic rms distribution about the mean coordinate positions (excluding residues 1-5 of each subunit) is 0.41 ± 0.08 Å for the backbone atoms and 0.90 ± 0.08 Å for all atoms. The three-dimensional solution structure of the IL-8 dimer reveals a structural motif in which two symmetry-related antiparallel α -helices, approximately 24 Å long and separated by about 14 Å, lie on top of a six-stranded antiparallel β -sheet platform derived from two three-stranded Greek keys, one from each monomer unit. The general architecture is similar to that of the $\alpha 1/\alpha 2$ domains of the human class I histocompatibility antigen HLA-A2. It is suggested that the two α -helices form the binding site for the cellular receptor and that the specificity of IL-8, as well as that of a number of related proteins involved in cell-specific chemotaxis, mediation of cell growth, and the inflammatory response, is achieved by the distinct distribution of charged and polar residues at the surface of the helices.

Communication between different cells of the immune system is achieved in part by a complex cascade of interacting proteins known as cytokines. The subject of the present study

is the cytokine interleukin 8 (IL-8)¹ [for a review, see Matsushima and Oppenheim (1989)], also known variously as

[†]This work was supported by the Intramural AIDS Targeted Antiviral Program of the Office of the Director of the National Institutes of Health (G.M.C. and A.M.G.).

[‡]Laboratory of Chemical Physics, NIDDK, NIH.

[§]Laboratory of Cell Biology, NCI, NIH.

^{||}Laboratory of Molecular Immunoregulation, National Cancer Institute.

[⊥]Research Laboratories, Dainippon Pharmaceutical Co.

¹ Abbreviations: IL-8, interleukin 8; MCAF, monocyte chemotactic and activating factor; PF4, platelet factor 4; GRO, growth-related gene product; MGSA, melanoma growth stimulating activity; γ IP-10, γ -interferon-induced protein; β TG, β -thromboglobulin; 9E3, chicken Rous sarcoma virus inducible protein; MHC, major histocompatibility complex; NOE, nuclear Overhauser effect; NOESY, two-dimensional nuclear Overhauser enhancement spectroscopy; PE-COSY, primitive exclusive two-dimensional correlated spectroscopy; SA, simulated annealing.

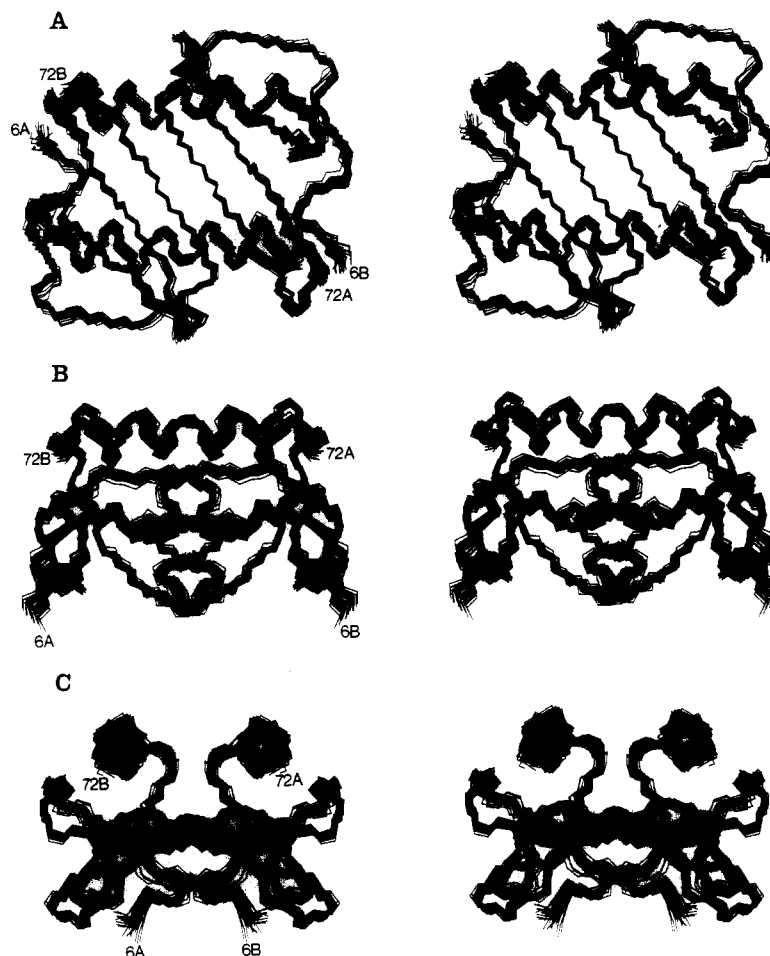


FIGURE 1: Three stereoviews showing best-fit superpositions of the backbone (N, C α , C) atoms of the 30 SA structures. The molecule is viewed down the C $_2$ symmetry axis in (A), which is located in the center of the β -sheet. The views in (B) and (C) are rotations about the C $_2$ axis which lies parallel to the plane of the paper.

neutrophil activation factor or protein (Walz et al., 1987), monocyte-derived neutrophil chemotactic factor (Yoshimura et al., 1987), and T-cell chemotactic factor (Larsen et al., 1989). IL-8 is a dimeric protein (Clore et al., 1989) composed of two identical subunits, each of $M_r \sim 8000$, which is released from several cell types, including monocytes, fibroblasts, endothelial cells, and keratinocytes, in response to an inflammatory stimulus. A range of in vitro and in vivo studies have shown that IL-8 possesses two major activities. The first is the selective capacity to attract neutrophils, basophils, and T-cells but not monocytes; the second involves neutrophil activation.

Sequence comparisons have revealed that IL-8 belongs to a superfamily of proteins involved in cell-specific chemotaxis, mediation of cell growth, and the inflammatory response. These include, among others, PF4, GRO/MGSA, γ IP-10, β TG, 9E3, RANTES, MCAF, and Act 2. All these proteins have four cysteine residues at approximately the same location in the amino acid sequence and have sequence homologies ranging from 20 to 35% for amino acid identity and up to 80% if conservative changes are taken into consideration, suggesting that they all have similar three-dimensional structures.

Recently, we presented the sequential assignment of the ^1H NMR spectrum of IL-8 and the delineation of elements of regular secondary structure (Clore et al., 1989). To gain a better understanding of the molecular basis of IL-8 activity, as well as of the factors contributing to different activities of the various related proteins, we have extended our previous work to the determination of the full three-dimensional structure of IL-8 in solution at high resolution by means of

NMR and hybrid distance geometry-dynamical simulated annealing calculations.

EXPERIMENTAL PROCEDURES

Recombinant IL-8 was expressed and purified as described by Furuta et al. (1989), and samples for NMR contained ~ 1.8 mM protein in either 99.996% D $_2$ O or 90% H $_2$ O/10% D $_2$ O at pH 5.2. All spectra were recorded at 600 MHz on a Bruker AM600 spectrometer at 40 $^\circ\text{C}$, and examples of the quality of the raw data are given in Clore et al. (1989).

NOEs were identified in 150-ms NOESY (Jeener et al., 1979) spectra and classified on the basis of 50- and 75-ms NOESY spectra into strong, medium, weak, and very weak, corresponding to interproton distance restraints of 1.8–2.7 \AA , 1.8–3.3 \AA (1.8–3.5 \AA for distances involving NH protons), 2.3–5.0 \AA , and 2.8–6.0 \AA , respectively. Upper limits for distances involving methyl protons or nonstereospecifically assigned methylene protons were corrected appropriately for center averaging (Wüthrich et al., 1983). In addition, 0.5 \AA was added to the upper limits for distances involving methyl protons (Clore et al., 1987).

Stereospecific assignments and ϕ , ψ , and χ_1 torsion angle restraints were derived from $^3J_{\text{HN}\alpha}$ and $^3J_{\alpha\beta}$ coupling constants (measured from PE-COSY spectra; Mueller, 1987) and intraresidue and sequential NOEs involving the NH, C $^\alpha$ H, and C $^\beta$ H protons by means of a conformational grid search with the program STEREOSEARCH (Nilges et al., 1990). The minimum ranges employed for the ϕ , ψ , and χ_1 torsion angles were $\pm 30^\circ$, $\pm 50^\circ$, and $\pm 20^\circ$, respectively (Kraulis et al., 1989).

Structures were computed by the hybrid distance geome-

Table I: Structural Statistics and Atomic rms Differences ^a

(A) Structural Statistics				
	(SA)	(SA)r		
RMS deviations from exptl distance restraints (Å) ^b				
all (1880)	0.031 ± 0.002	0.029		
intrasubunit				
interresidue short range ($ i - j < 5$) (784)	0.019 ± 0.002	0.020		
interresidue long range ($ i - j > 5$) (370)	0.027 ± 0.003	0.026		
intraresidue (540)	0.044 ± 0.002	0.042		
H-bond (104) ^c	0.031 ± 0.003	0.028		
intersubunit				
interproton (70)	0.022 ± 0.008	0.014		
H-bond (12) ^c	0.004 ± 0.006	0.000		
RMS deviations from exptl dihedral restraints (deg) (362) ^b				
F_{NOE} (kcal·mol ⁻¹) ^d	53 ± 5	48		
F_{tor} (kcal·mol ⁻¹) ^d	0.94 ± 0.36	0.98		
F_{sym} (kcal·mol ⁻¹) ^d	0.15 ± 0.04	424		
F_{repel} (kcal·mol ⁻¹) ^d	38 ± 4	37		
$E_{\text{L-J}}$ (kcal·mol ⁻¹) ^e	-542 ± 12	-474		
deviations from idealized geometry				
bonds (Å) (2392)	0.006 ± 0	0.011		
angles (deg) (4362)	2.016 ± 0.002	2.458		
impropers (deg) (882)	0.504 ± 0.010	0.485		
(B) Atomic rms Differences (Excluding Residues 1-5) (Å)				
	dimer		monomer	
	backbone atoms	all atoms	backbone atoms	all atoms
$\langle \text{SA} \rangle$ vs $\overline{\text{SA}}$	0.41 ± 0.08	0.90 ± 0.08	$\langle \text{SA}_a \rangle$ vs $\overline{\text{SA}}_a$	0.34 ± 0.06
$\langle \text{SA} \rangle_r$ vs $\overline{\text{SA}}$	0.19	0.44		0.86 ± 0.07
$\langle \text{SA} \rangle$ vs $\langle \text{SA} \rangle_r$	0.46 ± 0.07	1.00 ± 0.08		

^aThe notation of the structures is as follows: $\langle \text{SA} \rangle$ are the 30 final dynamical simulated annealing structures; $\overline{\text{SA}}$ is the mean structure obtained by averaging the coordinates of the 30 individual SA dimer structures best fitted to each other (excluding the N-terminal residues 1-5 of both subunits); $\langle \text{SA} \rangle_r$ is the restrained minimized mean structure obtained by restrained minimization of $\overline{\text{SA}}$; $\langle \text{SA}_a \rangle$ are the coordinates of the SA structures for one subunit only; $\overline{\text{SA}}_a$ is the mean structure for a single subunit obtained by averaging the coordinates of one subunit of the 30 SA structures best fitted to residues 6-72 of a single subunit. The number of terms for the various restraints is given in parentheses. The simulated annealing protocol is identical with that described by Nilges et al. (1988) with the exception of minor differences involving the use of dihedral angle restraints for ϕ , ψ , and χ_1 and a symmetry restraint. ^bNone of the structures exhibited distance violations greater than 0.3 Å or dihedral angle violations greater than 3°. ^cFor each backbone hydrogen bond there are two restraints: $r_{\text{NH-O}}$, 1.7-2.3 Å; $r_{\text{N-O}}$, 2.4-3.3 Å. Although these were identified on the basis of a qualitative interpretation of the NOE and NH exchange data, they were only included as restraints after they could be unambiguously assigned following the initial structure calculations. ^dThe values of the square-well NOE and torsion angle potentials [cf. eqs 2 and 3 in Clore et al. (1986)] are calculated with force constants of 50 kcal·mol⁻¹·Å⁻² and 200 kcal·mol⁻¹·rad⁻², respectively. E_{sym} is an effective harmonic potential used to maintain symmetry between the two subunits (Brünger, 1988) with a force constant set to 300 kcal·mol⁻¹·Å⁻² throughout the simulated annealing calculations. The atomic rms difference between the two subunits for the individual SA structures is less than 0.0008 Å for all atoms, while that for the restrained minimized mean structure ($\overline{\text{SA}}$)_r is 0.049 Å for all atoms and 0.001 Å for the backbone atoms. The value of the quartic van der Waals repulsion term [cf eq. 5 in Nilges et al. (1988)] is calculated with a force constant of 4 kcal·mol⁻¹·Å⁻⁴ with the hard-sphere van der Waals radii set to 0.8 times the standard values used in the CHARMM empirical energy function. ^e $E_{\text{L-J}}$ is the Lennard-Jones van der Waals energy calculated with the CHARMM (Brooks et al., 1983) empirical energy function. It is *not* included into the target function for simulated annealing.

try-dynamical simulated annealing method of Nilges et al. (1988) with a few minor modifications, making use of the programs DISGEO (Havel, 1986) and XPLOR (Brünger, 1988). An iterative approach to the structure determination was employed by carrying out a series of calculations with more and more restraints incorporated at each successive stage (Kraulis et al., 1989). This is particularly valuable for the identification of intersubunit NOEs involving side chains. As an example, consider the following NOEs between Ala-69 (C^βH₃) and Thr-37 (C^γH₃), Phe-65 (C^αH) and Ile-28 (C^αH), and Leu-25 (C^βH) and Val-27 (C^βH). The distances in the initial low-resolution structures between these protons were ~18, ~15, and ~8 Å, respectively, within each monomer, while the corresponding values for the intersubunit distances were all less than 4 Å. Given that NOEs, in the absence of extensive spin diffusion, are only observed for interproton distance separations less than 5 Å, it is evident that the observed NOEs between these three pairs of protons must arise from intersubunit contacts. Proceeding in this manner, the assignment of intersubunit NOEs was relatively straightforward.

The total number of experimental restraints used in the final calculations was 2242 for the dimer. These comprised a total of 1694 interproton distance, 104 hydrogen bonding, and 362

torsion angle restraints (involving 136 ϕ , 122 ψ , and 104 χ_1 angles) for the two subunits combined and 70 interproton distance and 12 hydrogen bonding restraints between the subunits. Stereospecific assignments were obtained for 38 of the 55 β -methylene groups per monomer and for the α -methylene groups of both glycine residues. The latter, as well as four of the β -methylene stereospecific assignments, could only be obtained after the initial rounds of calculations.

RESULTS AND DISCUSSION

Converged Structures. A total of 30 final simulated annealing (SA) structures were computed. The structural statistics are given in Table I, and superpositions of the N, C^α, and C backbone atoms are shown in Figure 1. Residues 1-5 of both subunits are poorly defined, as no sequential NOEs were observed for the first three residues and only ($i, i + 1$) sequential NOEs were observed from residue 3 to residue 6. The remainder of the structure, however, is exceptionally well determined with an overall atomic rms difference (excluding residues 1-5) between the individual dimer SA structures and the mean coordinate positions of 0.41 ± 0.08 Å for the backbone atoms and 0.90 ± 0.08 Å for all atoms (Figure 2A). The average angular rms difference for the ϕ and ψ torsion angles is 8.7 ± 5.9°, and the backbone torsion angles for all

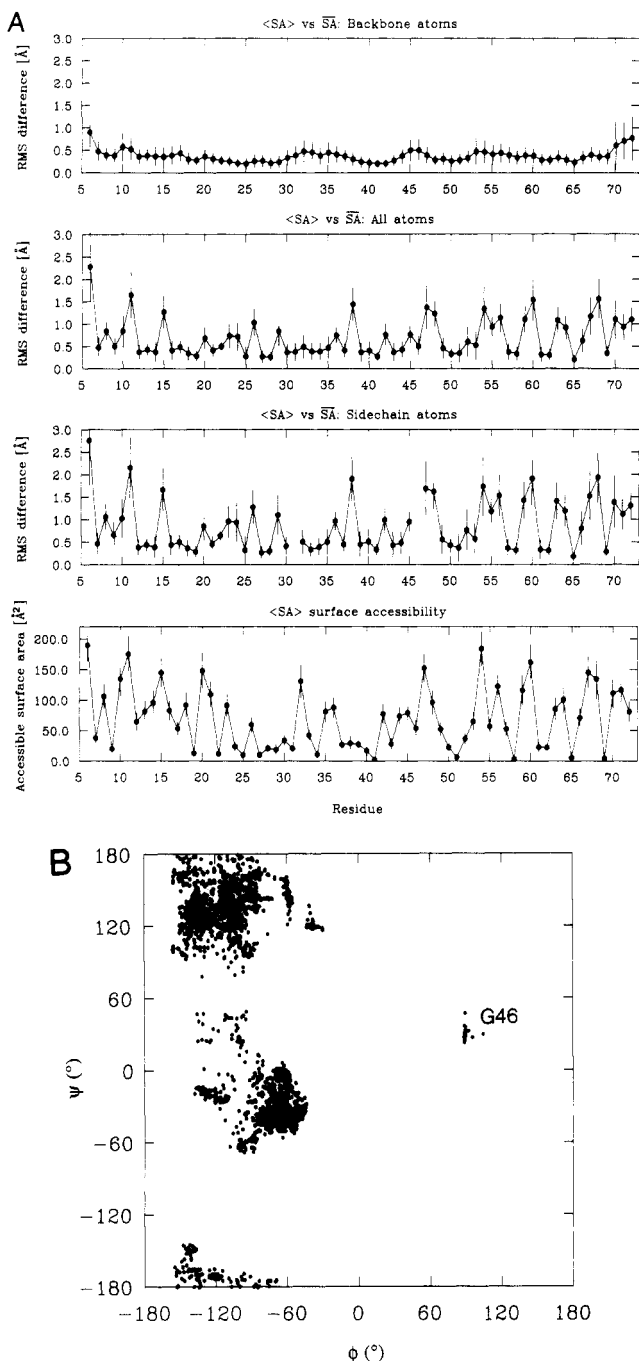


FIGURE 2: (A) Atomic rms distribution of the 30 individual SA structures about the mean structure \bar{SA} , together with the variation in surface accessibility as a function of residue number (excluding residues 1–5). The filled-in circles represent the average values at each residue and the bars the standard deviations in these values. (B) Ramachandran ϕ, ψ plot for the 30 SA structures (excluding residues 1–5). In both (A) and (B) the values are averaged over the two subunits.

non-glycine residues lie in the allowed region of a Ramachandran ϕ, ψ plot (Figure 2B). The majority of side-chain positions are also well-defined (Figures 2A and 3). Eighteen side chains, however, have atomic rms distributions about the mean coordinate positions larger than 1 Å. All of these are highly solvent accessible, and in the case of eight of them (Lys-11, Lys-15, Glu-38, Glu-48, Lys-54, Asn-56, Arg-60, and Glu-63), the $^3J_{\alpha\beta}$ coupling constants ($^3J_{\alpha\beta_2} \sim ^3J_{\alpha\beta_3} \sim 6\text{--}7$ Hz) are indicative of multiple χ_1 side-chain conformations. With the exception of Arg-6 and Arg-26, the remaining ill-defined side chains are located at the surface of the C-terminal α -helix. The χ_1 torsion angles of these residues are well defined but

the χ conformations beyond the C^β positions are poorly defined. The majority of these side chains comprise Lys and Arg residues. In contrast, most of the internal side chains have atomic rms distributions about the mean coordinate positions of ≤ 0.5 Å.

Description of the IL-8 Structure. Three views of the overall polypeptide fold are shown in Figure 1. The approximate overall dimensions of the IL-8 dimer (excluding side chains) are 30 Å long, 26 Å wide, and 18 Å deep in the view shown in Figure 1A. The structure essentially consists of two antiparallel α -helices lying on top of a six-stranded antiparallel β -sheet. The surface under the β -sheet is concave and except for Ile-28 and Ile-40 is composed entirely of hydrophilic and charged residues. The two symmetry-related helices are ~ 24 Å long and separated by a center to center distance of ~ 14 Å. The angle ($\sim 172^\circ$) between the long axes of the two helices is slightly less than 180° due to the right-handed twist of the β -sheet below (defined in terms of the twist of the peptide plane as viewed along the direction of a strand), and in particular of strand 1 of one subunit and strand 1' of the other.

The overall structure of the IL-8 dimer is similar to that of the AB dimer in the recently determined 3 Å resolution crystal structure of the PF4 tetramer (St. Charles et al., 1989); in particular, the arrangement of the β -sheet and α -helices is essentially identical. A detailed comparison between IL-8 and PF4 is not possible at the present time, since the coordinates of the PF4 structure have not yet been deposited in the Brookhaven Protein Data Bank and the structure has only been refined to an R factor of 28% (St. Charles et al., 1989). It is clear, however, that there are several noticeable structural differences between IL-8 and PF4, even at the level of the detailed secondary structure (Clare et al., 1989).

The topology and hydrogen-bonding pattern determined for IL-8 are depicted schematically in Figure 4. Within each subunit, the main secondary structure elements comprise a long C-terminal helix extending from residue 56 to residue 72 and a triple-stranded antiparallel β -sheet arranged in a Greek key, in which strand 1 (residues 23–30) is hydrogen bonded to strand 2 (residues 36–43), which in turn is hydrogen bonded to strand 3 (residues 48–51). The disulfide bridge between Cys-7 and Cys-34 is right-handed, while that between Cys-9 and Cys-50 is left-handed. At the N-terminus a series of nonclassical turns at residues Gln-8/Cys-9, Ile-10/Lys-11, and Ser-14 make up a long loop extending from Gln-8 to His-18. This is followed by a single 3-10 helical turn formed by residues 19–22, which leads into strand 1. Strands 1 and 2 are connected by a rather unusual turn or loop with a kink at Ser-30 and Ala-35 and two hydrogen bonds between the backbone amides of Gly-31 and Cys-34 and the carbonyl oxygen atoms of Cys-34 and Gly-31, respectively. The glycine at position 31 is either conserved or substituted conservatively by a serine in all members of the IL-8 family of proteins. A search of a database of high-resolution X-ray structures using the algorithm of Jones and Thirup (1986) revealed that the backbone atoms of residues 30–35 of IL-8 can be superimposed with an atomic rms difference of less than 0.5 Å on residues 56–61 of *Chromatium* high-potential iron protein and residues 96–101 of bovine trypsin. The conformation of the turn (residues 43–47) connecting strands 2 and 3 is also rather unusual and falls into the classification of a 3:5 type I turn with a G1 β -bulge (Sibanda & Thornton, 1985). In this regard, the backbone polypeptide chain of residues 42–48 can be superimposed within 0.5 Å on residues 78–84 of penicillopepsin, residues 24–30 of ovomucoid third domain, residues

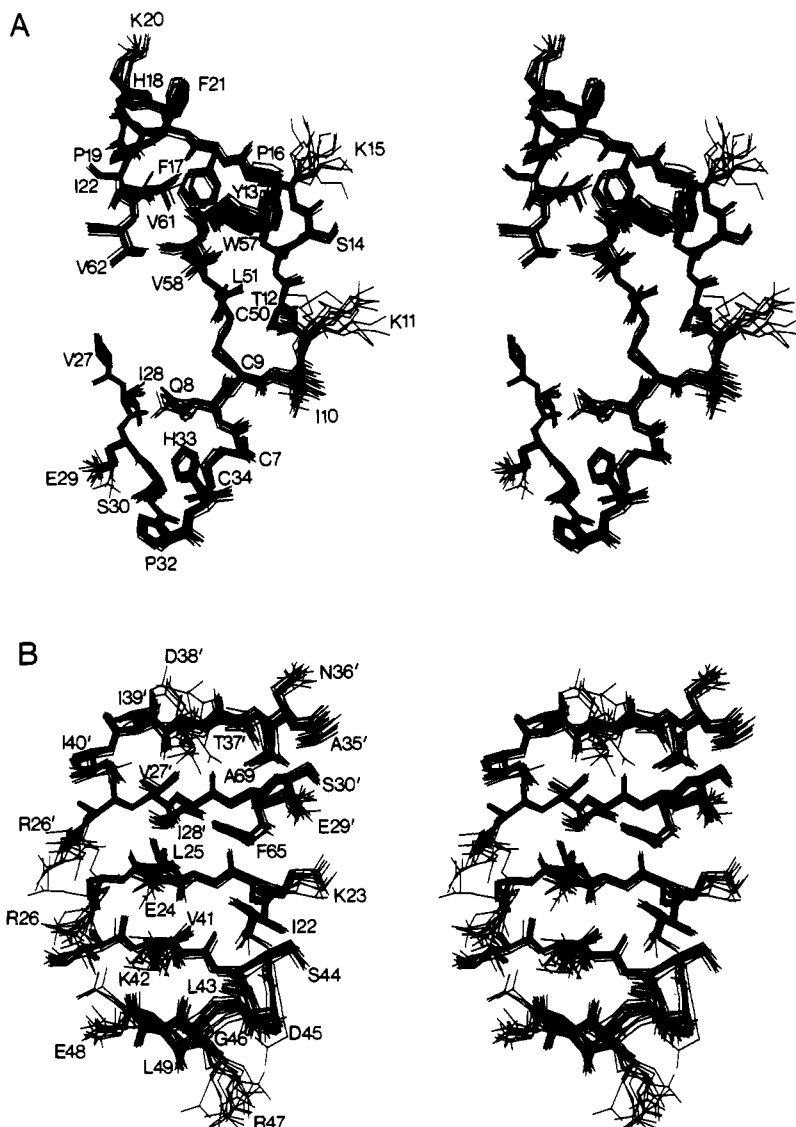


FIGURE 3: Stereoviews showing best-fit superpositions of all atoms (excluding protons) of 15 SA structures for two selected segments of the protein.

216–222 of bovine liver rhodanese, and residues 6–12 of plastocyanin. All of these structures have either a glycine or an asparagine at position 4 of the turn. The equivalent residue in IL-8 is Gly-46, which is conserved in PF4, β -TG, GRO/MGSA, and γ IP-10 and substituted conservatively by either an asparagine or a serine in the other members of the family. Strand 3 leads into the helix via a type I turn from residues 52–55 which is stabilized by two hydrogen bonds: a backbone NH(Glu-55)–CO(Asp-52) hydrogen bond and a hydrogen bond between the backbone amide of Lys-54 and the carboxylate side-chain group of Asp-52. The segment of residues 51–57 can be superimposed within 0.5 Å on residues 212–218 of penicillopepsin and residues 42–48 of reduced cytochrome c_2 .

The two histidine residues at positions 18 and 33 are highly unusual in so far that they have extremely low pK_a values of 3.7 and 4.9, respectively. The pK_a values for the majority of histidines reported to date have ranged between 5.5 and 7.5, with free histidine having a pK_a of ~ 6.5 (Jardetzky & Roberts, 1981). These findings can be rationalized in structural terms, since NH–N hydrogen bonds between a backbone amide proton and an imidazole ring nitrogen are observed for both histidines (Figure 3A). In the case of His-18 there is a hydrogen bond between the amide proton of Lys-20 and the

$N^{\delta 1}$ imidazole atom, while for His-33 the hydrogen bond is between the backbone amide proton of Gln-8 and the $N^{\epsilon 2}$ imidazole atom. The latter is unusual, as it represents the minor tautomeric form of free histidine. In addition, both the hydrogen bonds account for the very low field shifts of the NH protons of Gln-8 and Lys-20, which resonate at 11.94 and 11.53 ppm, respectively. This strong deshielding of the NH nucleus is caused by a downfield ring current shift due to the fact that the NH proton lies directly in the plane of the imidazole ring, possibly supplemented by an electric field effect from the polarizable imidazole ring. These two interactions may play an important role in stabilizing parts of the structure. In the case of His-18, the hydrogen-bonding interaction serves to stabilize the turn from residues 19–22, while in the case of His-33 it helps to maintain the spatial proximity between the 31–34 turn and residues 7 and 9 at the N-terminus. The latter may facilitate the formation of the disulfide bridge between Cys-7 and Cys-34 during protein folding. It is also interesting to note that His-33 is conserved in PF4, β TG, and GRO/MGSA.

The orientation of the helix relative to the triple-stranded β -sheet within each monomer is stabilized by a number of hydrophobic interactions (Figure 3). The six-membered ring of Trp-57 is perfectly stacked on top of the ring of Pro-16

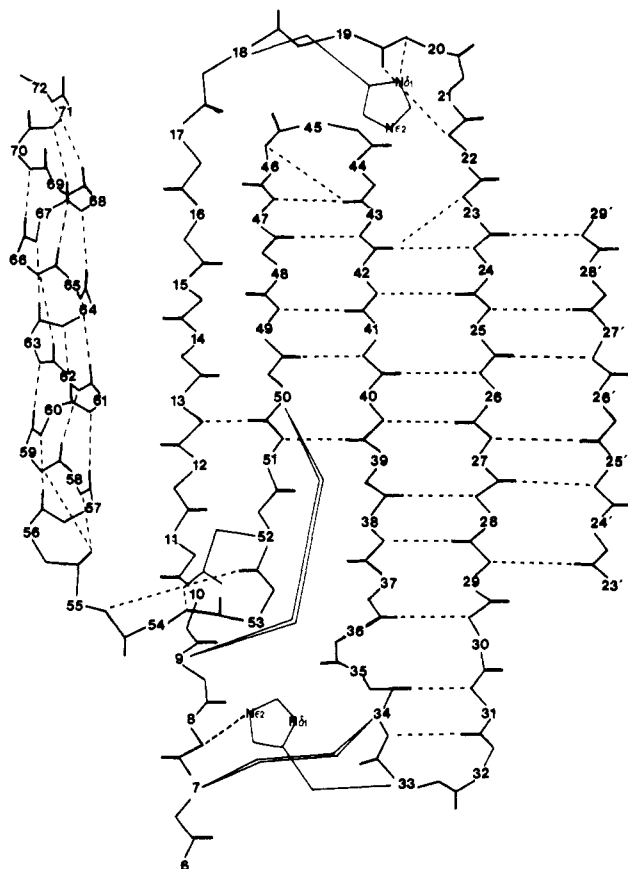


FIGURE 4: Schematic representation of the overall topology and hydrogen-bonding pattern in IL-8 deduced from analysis of the SA structures. All the residues of one subunit and residues 23'–29' of the second are shown. The diad axis lies between the C α atom positions of Arg-26 of the two subunits. Hydrogen bonds are indicated by dashed lines, and residue numbers are indicated at the C α atom positions.

(Figure 3A), accounting for the unusually high field shifted C α H resonance of Pro-16 which resonates at 1.63 ppm, as well as for the upfield shifts of the C β H and C γ H resonances. Trp-57 is also in close contact with Tyr-13, Phe-17, and Leu-51. Additionally, Phe-65 is in van der Waals contact with Pro-19, Ile-22, and Leu-25, Val-58 with Ile-39 and Leu-51, Val-61 with Pro-19, and Val-62 with Ile-22.

The dimer interface is principally stabilized by an antiparallel β -sheet with six hydrogen bonds between strand 1 from one subunit and strand 1' of the second (Figure 4). In addition, there are a number of other stabilizing forces involving side chains. There are hydrophobic contacts between Phe-65 of the C-terminal helix of one subunit and the methyl groups of Val-27 and the γ -methylene group of Glu-29 of the second and between Ala-69 of one subunit and Val-27 and Thr-37 of the second (Figure 3B). There is also an electrostatic interaction between the two helices involving Gln-59 of one subunit and Glu-70 of the other. These interactions further serve to maintain the orientation of the C-terminal helices, with respect both to each other and to the β -sheet below. The upper surface of the β -sheet that is in contact with one face of the α -helices is entirely hydrophobic, and there are hydrophobic interactions between residues of strand 1 from the two subunits, in particular between Leu-25 of one subunit and Val-27 of the other. Finally, there is an electrostatic interaction on the bottom of the β -sheet between Glu-24 of one subunit and Arg-26 of the other. It should be noted that these electrostatic interactions are not artifacts of the calculations as *no* electrostatic terms are used.

Relationship of Structure to Function. We have shown that the structure of IL-8 dimer consists of a six-stranded antiparallel β -pleated sheet that is spanned by the two long symmetry-related α -helices at the carboxy terminus of the two subunits. These helices are positioned at an angle of about $+60^\circ$ with respect to the orientation of the β -strands in the sheet and are separated by $\sim 14 \text{ \AA}$ (center to center). This architecture is closely related to the fold of the $\alpha 1/\alpha 2$ domains of the class I MHC antigen HLA-A2 determined by X-ray crystallography (Bjorkman et al., 1987), where the sheet is formed by eight β -strands, four from each domain, with two helices separated by $\sim 18 \text{ \AA}$ running across them at an angle of about -45° . [Further, the fold of the $\alpha 1/\alpha 2$ domains has been used to model the structure of the $\alpha 1/\beta 1$ intermolecular dimer of the class II MHC molecules (Brown et al., 1988).] Thus the same kind of general architecture is achieved with two different kinds of β -pleated sheets in which the strands run almost orthogonal to each other. In the case of HLA-A2, the β -sheet is formed by strands arising from two domains of a single subunit (i.e., a pseudodimer), while in the case of IL-8 and putatively the class II MHC molecules it is formed by strands originating from two separate subunits (i.e., an intermolecular dimer).

The views of the IL-8 structure presented in Figure 1 clearly demonstrate the prominent positioning of the two α -helices which sit on top of the rather flat β -sheet domain, with hydrophobic amino acid side chains forming the central features in the α/β interface. Indeed, this α -helix represents an almost idealized amphiphilic helix, with hydrophobic residues on the interior face and hydrophilic residues on the solvent-exposed face. The hydrophobic residues oriented toward the β -sheet are Val-58, Val-61, Val-62, and Phe-65 with the latter forming the central anchor of the helix. Leu-66 is located between the two helices while Trp-57 is involved in a stabilizing interaction between the loop around Pro-16 and the other side of the helix. The charged or polar amino acids that are solvent exposed are Asn-56, Gln-59, Arg-60, Glu-63, Lys-64, Lys-67, Glu-70, and Asn-71. The distribution of the different amino acids around the helix is illustrated in a helical wheel representation in Figure 5. In addition to the sequence of IL-8, a variety of sequences of related proteins have been included in this figure, with the alignment based on the assumption that the structure following Cys-50, as well as the phase of the helix, is similar in all the proteins. Although there is only structural data for two members of this family, namely, IL-8 and PF4 (St. Charles et al., 1989), it is evident from this illustration that, in all likelihood, the whole protein family contains the same structural feature at this position in the sequence. All the sequences exhibit amphiphilic properties of a potential α -helix with strong conservation of hydrophobic residues for those positions that are found at the α/β interface in IL-8 and PF4.

In light of the structural similarities between the $\alpha 1/\alpha 2$ domains of HLA-A2 and IL-8, it is tempting to speculate on the functional role of the long helix in IL-8. In HLA-A2 the antigen recognition site and T-cell receptor interaction is believed to reside in the region between and comprising two approximately antiparallel α -helices (Bjorkman et al., 1987). While the $\alpha 1$ and $\alpha 2$ domains of HLA-A2 are not identical, they are similar, and the two helices are related by a pseudodimer. In the case of IL-8, the two subunits are identical, and the two α -helices are located symmetrically about the diad axis. It therefore may well be that the two long α -helices in IL-8 and the other related proteins serve as a major interaction site with the respective receptor. This hypothesis is particularly attractive as a C-terminal tridecapeptide of PF4 comprising

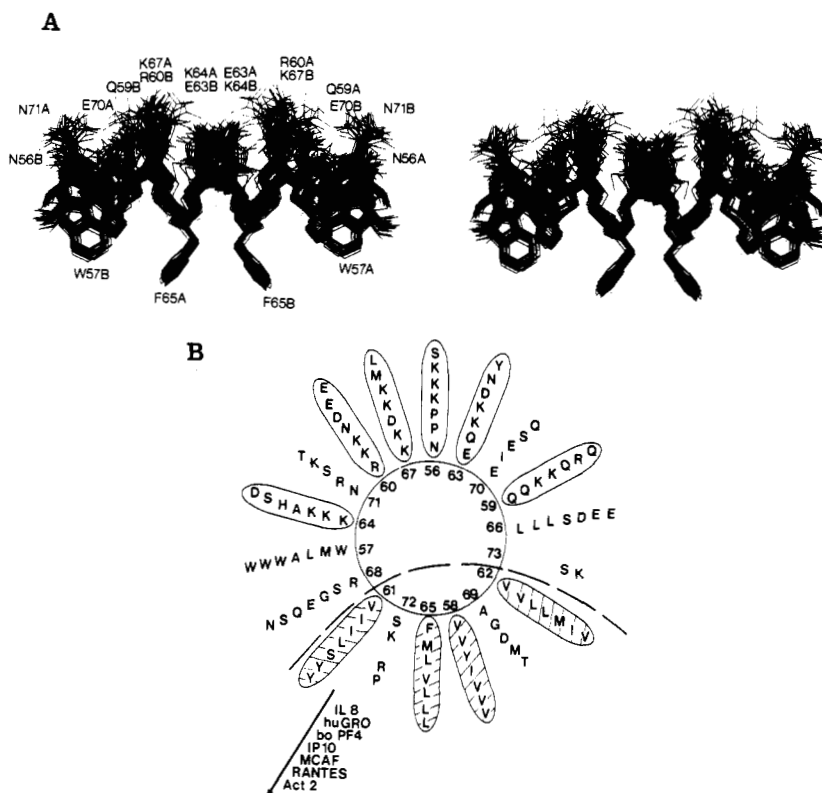


FIGURE 5: (A) Stereoview showing a best-fit superposition of all atoms (excluding protons) of the 30 SA structures for the helical residues (56–72) of both subunits. The view of the helices is the same as that in Figure 1B. (B) Helical wheel representation of the C-terminal helix together with its sequence in IL-8 and its putative sequence in some related proteins. The hydrophobic and hydrophilic faces are separated by a dashed line. The polar and charged surface residues are encircled, while the hydrophobic residues that interact with the β -sheet are encircled and shaded.

residues 56–68 (numbering of IL-8) has both chemotactic (Deuell et al., 1981) and immunoregulatory (Zucker et al., 1989) activity. Specific recognition would then be achieved primarily through the different combinations of polar and charged residues on the outside of the helix which would have their counterparts on the surface of the cellular receptor. In particular, the residues that are likely to be important are located at positions 59, 60, 63, 64, and 67. In this regard it is interesting to note that GRO/MGSA binds to the same receptor on human neutrophils as IL-8; concomitantly, IL-8 shows significant melanoma stimulating activity (Matsushima & Oppenheim, 1989). Examination of Figure 5 reveals that the only changes in any of these residues are conservative (Arg-60 \rightarrow Lys and Glu-63 \rightarrow Gln), preserve functional groups, and do not cause any charge reversal. In contrast, PF4 does not bind to the IL-8 receptor, which may possibly be accounted for by an alteration in charge at positions 63 (Glu \rightarrow Lys) and 67 (Lys \rightarrow Asp). Similarly, the single charge inversion at position 61 (Arg \rightarrow Asp), coupled with the replacement of the $N^H_3^+$ functional group of Lys-64 by the imidazole ring of a histidine, may account for the differential chemotactic specificity of MCAF and IL-8, the former for monocytes and the latter for neutrophils, basophils, and T-cells. Finally, we note that the distinct distribution and pattern of charged residues at the surface of the two symmetry-related helices form an ideal template for the design of potential IL-8 inhibitors which would act by binding to the shallow groove between the two helices, thereby preventing the interaction of IL-8 with its cellular receptor.

SUPPLEMENTARY MATERIAL AVAILABLE

The coordinates of the 30 SA structures of the IL-8 dimer, as well as those of the restrained minimized mean structure

(SA)r, together with the complete list of experimental restraints have been deposited in the Brookhaven Protein Data Bank.

REFERENCES

- Bjorkman, P. J., Saper, M. A., Samraoui, B., Bennett, W. S., Strominger, J. L., & Wiley, D. C. (1987) *Nature (London)* 329, 506–512.
- Brooks, B. R., Bruccoleri, R. E., Olafson, B. D., States, D. J., Swaminathan, S., & Karplus, M. (1983) *J. Comput. Chem.* 4, 187–217.
- Brown, J. H., Jardetzky, T., Saper, M. A., Samraoui, B., Bjorkman, P. J., & Wiley, D. C. (1988) *Nature (London)* 332, 845–850.
- Brünger, A. T. (1988) *XPLOR Manual*, Yale University, New Haven, CT.
- Clore, G. M., Nilges, M., Sukumaran, D. K., Brünger, A. T., Karplus, M., & Gronenborn, A. M. (1986) *EMBO J.* 5, 2729–2735.
- Clore, G. M., Gronenborn, A. M., Nilges, M., & Ryan, C. A. (1987) *Biochemistry* 26, 8012–8023.
- Clore, G. M., Appella, E., Yamada, M., Matsushima, K., & Gronenborn, A. M. (1989) *J. Biol. Chem.* 264, 18907–18911.
- Deuell, T. F., Senior, R. M., Chang, D., Griffin, G. L., Heinrichson, R. L., & Kaiser, E. T. (1981) *Proc. Natl. Acad. Sci. U.S.A.* 78, 4854–4857.
- Furuta, R., Yamagishi, J., Kotani, H., Sakamoto, F., Fukui, T., Matsui, Y., Sohmura, Y., Yamada, M., Yoshimura, T., Larsen, C. G., Oppenheim, J. J., & Matsushima, K. (1989) *J. Biochem. (Tokyo)* 106, 436–441.
- Havel, T. F. (1986) *DISGEO*, Quantum Chemistry Program Exchange No. 507, Indiana University, Bloomington, IN.

- Jardetzky, O., & Roberts, G. C. K. (1981) *NMR in Molecular Biology*, Academic Press, New York.
- Jeener, J., Meier, B. H., Bachmann, P., & Ernst, R. R. (1979) *J. Chem. Phys.* 71, 4546-4553.
- Jones, T. A., & Thirup, S. (1986) *EMBO J.* 5, 819-822.
- Kraulis, P. J., Clore, G. M., Nilges, M., Jones, T. A., Pettersson, G., Knowles, J., & Gronenborn, A. M. (1989) *Biochemistry* 28, 7241-7257.
- Larsen, C. G., Anderson, A. O., Appella, E., Oppenheim, J. J., & Matsushima, K. (1989) *Science (Washington, D.C.)* 243, 1464-1467.
- Matsushima, K., & Oppenheim, J. J. (1989) *Cytokine* (in press).
- Mueller, L. (1987) *J. Magn. Reson.* 72, 191-196.
- Nilges, M., Clore, G. M., & Gronenborn, A. M. (1988) *FEBS Lett.* 229, 317-324.
- Nilges, M., Clore, G. M., & Gronenborn, A. M. (1990) *Biopolymers* (in press).
- Sibanda, B. L., & Thornton, J. M. (1985) *Nature (London)* 316, 170-174.
- St. Charles, R., Walz, D. A., & Edwards, B. F. P. (1989) *J. Biol. Chem.* 264, 2092-2099.
- Walz, A., Peveri, P., Aschauer, H., & Baggolini, M. (1987) *Biochem. Biophys. Res. Commun.* 149, 755-761.
- Wüthrich, K., Billetter, M., & Braun, W. (1983) *J. Mol. Biol.* 169, 949-961.
- Yoshimura, T., Matsushima, K., Tanaka, S., Robinson, E. A., Appella, E., Oppenheim, J. J., & Leonard, E. (1987) *Proc. Natl. Acad. Sci. U.S.A.* 84, 9233-9237.
- Zucker, M. B., Katz, I. R., Thorbecke, G. J., Milot, D. C., & Holt, J. (1989) *Proc. Natl. Acad. Sci. U.S.A.* 86, 7571-7524.

Methane Monooxygenase Catalyzed Oxygenation of 1,1-Dimethylcyclopropane. Evidence for Radical and Carbocationic Intermediates[†]

Frank Ruzicka,[‡] Ded-Shih Huang,[‡] Mark I. Donnelly,[§] and Perry A. Frey*[‡]

Institute for Enzyme Research, Graduate School, and Department of Biochemistry, College of Agricultural and Life Sciences, University of Wisconsin—Madison, Madison, Wisconsin 53705, and Amoco Research Center, Naperville, Illinois 60566

Received December 11, 1989

ABSTRACT: Methane monooxygenase catalyzes the oxygenation of 1,1-dimethylcyclopropane in the presence of O₂ and NADH to (1-methylcyclopropyl)methanol (81%), 3-methyl-3-buten-1-ol (6%), and 1-methylcyclobutanol (13%). Oxygenation by ¹⁸O₂ using the purified enzyme proceeds with incorporation of ¹⁸O into the products. Inasmuch as methane monooxygenase catalyzes the insertion of O from O₂ into a carbon-hydrogen bond of alkanes, (1-methylcyclopropyl)methanol appears to be a conventional oxygenation product. 3-Methyl-3-buten-1-ol is a rearrangement product that can be rationalized on the basis that enzymatic oxygenation of 1,1-dimethylcyclopropane proceeds via the (1-methylcyclopropyl)carbinyl radical, which is expected to undergo rearrangement with ring opening to the homoallylic 3-methyl-3-buten-1-yl radical in competition with conventional oxygenation. Oxygenation of the latter radical gives 3-methyl-3-buten-1-ol. 1-Methylcyclobutanol is a ring-expansion product, whose formation is best explained on the basis that the 1-methylcyclobutyl tertiary carbocation is an oxygenation intermediate. This cation would result from rearrangements of carbocations derived by one-electron oxidation of either radical intermediate. The fact that both 3-methyl-3-buten-1-ol and 1-methylcyclobutanol are produced suggests that the oxygenation mechanism involves both radical and carbocationic intermediates. Radicals and carbocations can both be intermediates if they are connected by an electron-transfer step. A reasonable reaction sequence is one in which the cofactor (μ-oxo)diiron reacts with O₂ and two electrons to generate a hydrogen atom abstracting species and an oxidizing agent. The hydrogen-abstracting species might be the enzymic radical or another species generated by the iron complex and O₂. Oxygenation then could proceed by abstraction of a hydrogen atom from the substrate to form a radical, followed by electron transfer from the radical to the oxidizing species to form a carbocation. The carbocation would be quenched by oxygen associated with the oxygenation cofactor to generate the product.

Methane monooxygenase catalyzes the oxygenation of methane in methanotrophic bacteria according to eq 1.¹ The

$$\text{H}^+ + \text{CH}_4 + \text{NADH} + \text{O}_2 \rightarrow \text{CH}_3\text{-OH} + \text{H}_2\text{O} + \text{NAD}^+ \quad (1)$$

enzymes from *Methylococcus capsulatus* (Bath) and *Methylosinus trichosporium* (OB3b) are complexes of the fol-

lowing three proteins: (a) An oxygenase designated as component A that contains a (μ-oxo)diiron complex and an organic radical. The oxygenase has an overall *M_r* of 220 000 and comprises three subunits of *M_r* 54 000, 42 000, and 17 000, respectively, with two copies of each subunit and two (μ-oxo)diiron complexes in each enzyme particle. (b) A flavo-

[†]Supported by a contract from the Amoco Corp. to the University of Wisconsin—Madison.

[‡]University of Wisconsin—Madison.

[§]Amoco Research Center.

¹ Abbreviations: NAD⁺, oxidized nicotinamide adenine dinucleotide; NADH, reduced nicotinamide adenine dinucleotide; MOPS, 3-(*N*-morpholino)propanesulfonic acid; NMR, nuclear magnetic resonance; GC, gas chromatography; GC-MS, gas chromatographic mass spectroscopy.